Preparation and characterization of F-, O-, and N-containing carbon nanoparticles for pH sensing

Vladyslav Lisnyak, Alexander Zaderko, Ruslan Mariychuk, Volodymyr Lysenko, Olga Yu. Boldyrieva, Valeriy Skryshevsky, Gauhar Mussabek, Yerzhan Taurbayev, Nazym Zhylkybayeva, Oksana Yu. Tananiko

Preparation and characterization of F-, O-, and N-containing carbon nanoparticles for pH sensing

Vladyslav Lisnyak, Alexander Zaderko, Ruslan Mariychuk, Volodymyr Lysenko, Olga Yu. Boldyrieva, Valeriy Skryshevsky, Gauhar Mussabek, Yerzhan Taurbayev, Nazym Zhylkybayeva, Oksana Yu. Tananiko

Applied Nanoscience
https://doi.org/10.1007/s13204-021-01725-7

ORIGINAL ARTICLE

Preparation and characterization of F-, O-, and N-containing carbon nanoparticles for pH sensing

Vladyslav V. Lisnyak[1,2] · Alexander N. Zaderko[3] · Ruslan Mariychuk[2] · Volodymyr Lysenko[4] · Olga Yu. Boldyrieva[1] · Valeriy A. Skryshevsky[3] · Gauhar Mussabek[5,6] · Yerzhan Taurbayev[5,6] · Nazym Zhylkybayeva[6] · Oksana Yu. Tananiko[1]

Received: 3 January 2021 / Accepted: 31 January 2021

Abstract

A novel sensing system was designed for pH measurements based on the enhanced and quenched photoluminescence (PL) and UV–Vis absorption of the diluted water solutions of F-, O-, and N-containing carbon nanoparticles (FON-CNPs). These FON-CNPs were solvothermally synthesized, dissolved, ultra-filtrated, and separated by thin-layer chromatography. The total fluorine content in them was found to be 1.2–1.5 mmol per gram. Their TGA showed a total weight loss of 52.7% because of the thermal decomposition and detachment of the surface groups and the partial burning of the functionalized shell on the carbon core at temperatures below 1200 °C. TEM and Raman data confirmed the presence of graphitic structures in the carbon core. From the results of ATR FTIR and UV–Vis spectroscopies, we showed that a carbon shell incorporates different functional groups covering the carbon core. The surface groups of the carbon shell include carboxyl, phenolic, and carbonyl groups. Heterocyclic N-containing and amino groups and trifluoromethyl groups supporting the hydrophobicity were also found. We suggested the possible reasons for the pH responses obtained with the sensing system considering them dependent on the de-protonation of functional groups with pH change.

Keywords F-,O- · and N-containing carbon NPs · Solvothermal synthesis · Photoluminescence · pH nanosensors

✉ Vladyslav V. Lisnyak
lisnyak@univ.kiev.ua

Alexander N. Zaderko
indeo1016@gmail.com

Ruslan Mariychuk
ruslan.mariychuk@unipo.sk

Volodymyr Lysenko
vladimir.lysenko@univ-lyon1.fr

Olga Yu. Boldyrieva
ob@univ.kiev.ua

Valeriy A. Skryshevsky
skryshevsky@gmail.com

Gauhar Mussabek
gauhar.musabek@kaznu.kz

Yerzhan Taurbayev
taurbayev@taur.kaznu.kz; taurbayev@mail.ru

Nazym Zhylkybayeva
naz-30@mail.ru

Oksana Yu. Tananiko
otananaiko@gmail.com

[1] Faculty of Chemistry, Taras Shevchenko National University of Kyiv, 64/13 Volodymyrs'ka Str., Kyiv 01601, Ukraine

[2] Department of Ecology, Faculty of Humanities and Natural Sciences, The University of Prešov in Prešov, 17th November Str. 1, 08001 Prešov, Slovakia

[3] Institute of High Technologies, Taras Shevchenko National University of Kyiv, 64, Volodymyrs'ka Street, Kyiv 01601, Ukraine

[4] Light Matter Institute, UMR-5306, Claude Bernard University of Lyon, 2 rue Victor Grignard, 69622 Villeurbanne, France

[5] Institute of Information and Computational Technologies, 125, Pushkin Str., Almaty 050000, Kazakhstan

[6] Faculty of Physics and Technology, Al-Farabi Kazakh National University, 71 Al-Farabi Ave., Almaty 050040, Kazakhstan

Introduction

Carbon nanoparticles (CNPs), including carbon dots (CDs), are of special attention in a broad range of applications because of their tunable optical properties and excellent biocompatibility (Xia et al. 2019; Sun et al. 2020; Nevar et al. 2020; Tarasenka et al. 2017; Zuo et al. 2018; Pal et al. 2020). These green and nontoxic carbonic nanomaterials were used as the fluorophores and absorbers. In case of an increase in the spectral overlap between absorbing species and fluorophore, one can see a decrease in fluorescence/photoluminescence intensity of NPs. This decrease is considered as a response and enables quantitative measurement of the adsorbents. Today, numerous publications are devoted to the application of CNPs as selective photoluminescence on–off–on probes (Novoa De León et al. 2019; Feng et al. 2019 Zan et al. 2020; Wang et al. 2019).

On the other hand, many semiconductors showed the photoluminescence (PL) intensity and decay lifetime strongly dependent on the value of pH. This pH dependence, in the case of porous Si, is explained by competition between UV-induced hydrogen effusion, hydrogen adsorption from the buffer solution, and surface oxidation. Within the phenomenon, pH sensors were already proposed (Benilov et al. 2007). Besides, when different luminescent NPs are storage in the porous Si and nanosilicas, they can be used as specific probe units in multicomponent sensors (Serdiuk et al. 2011; He et al. 2020).

Despite a wide variety of CNPs, the fluorine and nitrogen-containing CNPs have rarely been used as effective pH sensors (Long et al. 2018; Su et al. 2019) and for other application until nowadays (Sim Y et al. 2019; Wang et al. 2019; Liu et al. 2019; Jiang et al. 2019).

In this work, we report on new fluorine-, oxygen-, and nitrogen-containing carbon nanoparticles (FON-CNP). They were obtained by a one-stage solvothermal method from citric acid, urea, and 3-(trifluoromethyl) aniline. The latter was applied as a source of fluorine and nitrogen. Here, citric acid and urea were pyrolyzed to form the carbon matrix. The resulting FON-CNPs have excellent water solubility and bright PL in aqueous solutions. Remarkably, the PL intensity and UV absorption of FON-CNP showed pH-dependent responses. The PL intensity maintains certain stability over a wide pH range of 1.0–11, showing good reversibility. Based on the pH-dependent behavior of FON-CNPs, one can create a sensor system for accurate pH measurements.

Experimental

Materials

3-(Trifluoromethyl)aniline (> 99%, CAS#98–16–8) provided by Merck was used for the preparation of the FON-CNPs. Pharmaceutical-grade anhydrous citric acid and pro-analysis quality urea were supplied by LLC Himlaborreaktiv (Brovary, Ukraine). LLC Himlaborreaktiv solvents, acids, bases, and reagents in the present study were of analytical purity and were used as received. For dilution, Millipore deionized water was used in the experiments. Phosphate-buffered (PB) solutions of different pH levels were prepared by titrating 0.01 mol L^{-1} phosphoric acid solution with 1 M NaOH solution to the required pH values. The preparation was carried out under control with a pH electrode (InLab Routine Pro, Mettler Toledo).

Synthesis of FON-CNPs

The samples of FON-CNPs were synthesized by the solvothermal method (Zaderko 2020). In a typical synthesis procedure, we had composed a mixture of 10 g of urea (0.167 mol), 16 g of anhydrous citric acid (0.083 mol), and 3.35 g of 3-(trifluoromethyl) aniline (0.021 mol). The mixture was placed in a glass reactor and left it open. The reactor with the mixture within was placed in an electric oven, which was heated from 25 to 135 °C for 30 min, and held at this temperature for the next 30 min to get a yellow melt from the stored mixture. After that, the reactor temperature was increased from 135 to 165 °C for 10–13 min. After 2 h of heat treatment at this temperature, the melt was transformed into a dark brown shining solid. 75 ml of an ethanol/water solution (50/50) was added to the reactor after the synthesis to dissolve the solid. The resulting dark brown solution was then filtered through Whatman filter paper and acidified by adding 20 ml of concentrated HCl. When HCl was added, FON-CNP flocks began to form in the solution. After holding for an hour, the precipitate was separated by vacuum filtration, and the resulting brownish powder was dried in the air.

Instrumentation

Fourier-transform infrared attenuation total reflectance (FTIR ATR) spectra were collected on a Shimadzu IRPrestige 21 instrument. A MIRacle module (Pike Technology), with a ZnSe crystal plate for the sample contact, was used during FTIR ATR measurements. Transmission electron microscopy (TEM) images were captured on an electronic microscope (Jeol JEM-2100F, 200 kV). Energy-dispersive X-ray (EDX) analysis of TEM imaged samples was carried out on an AZtec X-MAX energy-dispersion spectrometer from Oxford Instruments. Ultraviolet–visible (UV–vis) absorption spectra were recorded by a UV–vis spectrophotometer (Varian Cary 50) at an UV–Vis scan rate of 600 nm min^{-1}. PL spectra of the solutions of FON-CNPs were measured at 20 °C on the Agilent Cary Eclipse fluorescence spectrophotometer (Xe flash lamp).

Thermogravimetric analysis (TGA) of dried samples was carried out in an argon gas flow with a custom instrument reported elsewhere (Tsapyuk et al. 2020). Measurements of the total fluoride content (C_F) were done in an aqueous solution prepared by pyrolytic decomposition of samples (Zaderko et al. 2019). The Mettler Toledo (SevenExcellence™) pH meter was used to measure pH levels with maximum measurement accuracy.

Raman spectrum of FON-CNPs was collected in backscattered mode with a HORIBA Jobin Yvon-LabRAM ARAMIS integrated confocal micro-Raman system equipped with a microscope (BX41, Olympus, Japan) and a diode-pumped solid-state laser. A 633 nm laser was focused by an Olympus 100× objective lens (UPLSAPO, NA = 0.95) on the sample placed in an open-air environment at room temperature. The excited Raman scattering signal was collected by a Labram ARAMIS (Jobin–Yvon) spectrometer.

Results and discussion

EDX analysis confirms the presence of fluorine, oxygen, carbon, and nitrogen in the FON-CNPs. According to the chemical analysis, the fluorine content C_F equals 1.2–1.5 mmol per gram. Figure 1a shows the formation of polydisperse agglomerates of monodisperse primary particles. Although the pseudo-spherical NPs are showed a wide range of size distribution, from 25 to 80 nm, the mean agglomerate diameter is about 55 ± 5 nm. The SAED pattern confirms the amorphous structure of the prepared agglomerated NPs (Fig. 1b).

The alcohol–water solutions of FON-CNPs (3 ml, 46 g of dry FON-CNPs/L in 37 wt/v% alcohol solution diluted with 2 mL of water) were subjected to ultrafiltration. Giving a brown solution, the ultra-filtration with 10 kDa membrane centrifugal filters showed that the FON-CNPs could be completely filtered for 3 h at 5500 g. To prepare the solution of FON-CNPs of the smallest molecular weight range, the prepared ultra-filtrate was diluted three times with water and filtered in sequence with centrifugal filters from Vivaspin and Microsep Omega, equipped with membranes with molecular weight cut-offs of 5 and 1 kDa, at 5000 g. The filtrates of 0.03 mass% solutions of FON-CNPs after filtering with a 1 kDa membrane showed yellow and white luminescence under 254 nm and 365 nm excitations, respectively (Fig. 1d). This confirms a bimodal luminescence nature in the alcohol–water solutions of FON-CNPs similar to that observed by Yang et al. (2020) for green–yellow emitting CDs derived from xylose and applied in the pH sensing.

After ultrafiltration, the resulting yellow solution to be used in subsequent experiments was subjected to thin-layer chromatography (TLC) with a silica layer (6 nm silica, 15 mkm). On the TLC plate after chromatographing, one can see two components, which exhibit blue and yellow luminescence under UV light (see insert in Fig. 1c).

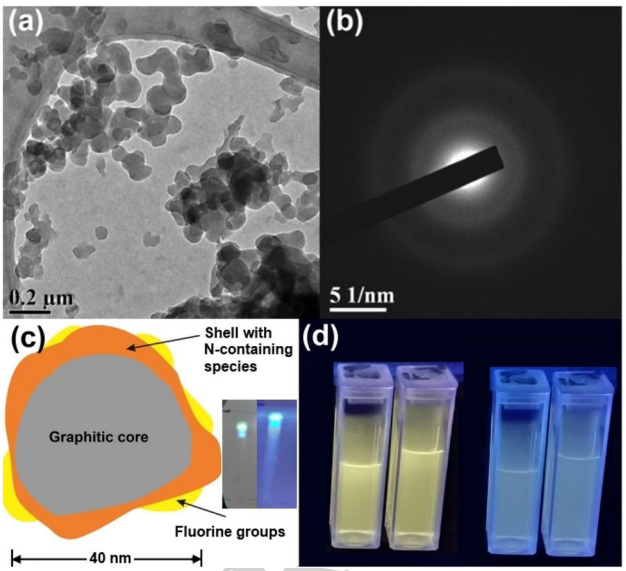

Fig. 1 **a** TEM image and **b** SEAD pattern of FON-CNPs agglomerated with HCl, **c** Suggested structure of NPs, **d** Photographs of FON-CNPs after 10 and 1 kDa filtering under 254 nm and 365 nm UV light (from left to right), Insert in **c** Completed chromatograms of FON-CNPs dissolved in 2:1 isopropanol-water solution on TLC plates photographed under UV lamp excitation

FTIR ATR spectrum (Fig. 2a) of FON-CNPs was registered for the sample, which was dried on a Parafilm™ M substrate. This spectrum confirmed the formation of different functional groups forming a shell on the surface. For all benzene derivatives containing CF_3 groups, an asymmetric C–F stretching vibration at 1330 cm^{-1} appears with very strong intensity (Yadav and Singh 1985). A band at 1553 cm^{-1} (C=N) and bands at 1611 and 1666 cm^{-1} (C=C) can be assigned to stretching vibrations in the aromatic rings of the carbon (N) skeleton (Rap et al. 2020). According to Singh and Yadav (2001), three mid-intensity bands peaked at 697 cm^{-1}, 797 cm^{-1}, and 890 cm^{-1} are due to the C–C–C in-plane bending mode, the symmetric C–F stretching vibration in the CF_3 group that mixed with the ring-breathing mode vibrations, and the out-of-plane C–H bending vibrations, correspondingly.

A band at 1128 cm^{-1} could be assigned to the N−H and C−H stretching vibrations. Unless otherwise stated, here and below the group frequencies are assigned according to Socrates (1994) and Coates (2006). Some spectral features are consistent with the formation of oxygen-containing groups. Two peaks centered at 1708 cm^{-1} and 1666 cm^{-1} are from C=O stretching vibrations of carbonyl groups (Bellamy 1980). A band at 1449 cm^{-1} corresponds to the C–N stretching vibrations or the overlapping bands assigned to the CH_2 scissoring and C–O–H bending vibrations.

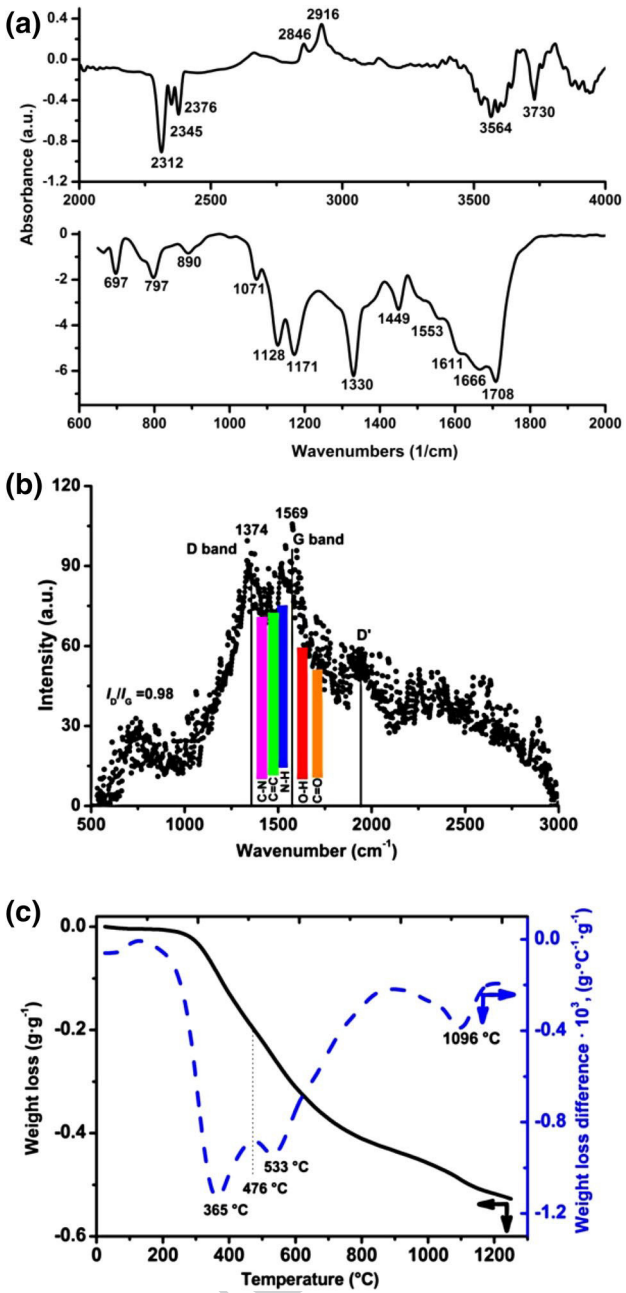

Fig. 2 Spectra **a** FTIR ATR and **b** Raman, and **c** TG analysis of FON-CNPs

The complex of spectral bands observed between 1500 and 1800 cm^{-1} includes the contribution of the NH_2 and CHN bending vibrations and that of CNH stretching vibrations. According to Larkin (2011), the quadrant ring and semi-circle stretching vibrations in heterocycles absorb in this spectral region. Broadband absorption in the region of 1000–1320 cm^{-1} covers the whole range of frequencies in which the C−OH, C−C, C−N, and C−O stretching vibrations are registered. A peak at 1071 cm^{-1} is from C−O stretching vibrations, and it can contain the isopropanol contribution (Coblentz Soc., Inc. 2018). While the broadband at 3200–3600 cm^{-1} could be assigned to the O−H stretching vibrations overlapped with N−H vibrational frequencies in aromatic and heterocyclic groups, and those of imino groups (Lin 2018). The reversed Christiansen peaks at 2916 cm^{-1} and 2846 cm^{-1} are attributed to asymmetrical and symmetrical stretching vibrations of – CH_2. These peaks are from isopropanol solvent (Shahravan et al. 2012) and Parafilm™ M substrate. According to Kauffman et al. (2011), three bands at 2312 cm^{-1}, 2345 cm^{-1}, and 2376 cm^{-1} are from adsorbed CO_2 surface species. Broadband with a peak at 3564 cm^{-1} could also include the contribution from defects forming hydroxyl and from isopropanol conformers (Coblentz Soc., Inc. 2018). In the highest wavenumber region, presumably, a peak at 3730 cm^{-1} could be assigned to free hydroxyl ions or the hydroxyl coverage of FON-CNPs. Besides, according to Larkin (2011), the combination band deriving from the bands involving the CO_2 in-phase stretching and out-of-phase stretch could be observed as two doublets in the 3730–3500 cm^{-1} range. Presumably, the reason for increasing the PL efficiency is the constitutional and shell nitrogen-containing groups.

Figure 2b shows the Raman spectrum of the sample, where the *D*, *G*, and *D′* bands are seen. In the present study, the width of the *D* band is very wide, reflecting the wide distribution of crystallite sizes. One should note that the ratio I_D/I_G equals 0.98, so by Cancado's general formula (Cancado et al. 2006), which allows the determination of the crystallite size L_a by Raman spectroscopy, the L_a value of 39.3 nm was calculated. A Raman peak at 1569 cm^{-1}, which is assigned to the *G* band of graphitic structures, can overlap with the abundant Raman bands, those vibrations most likely assigned to the bending – OH vibrations, deformation N–H vibrations, ring C=C vibrations, and C=O and C–N stretching vibrations (Lin-Vien et al. 1991; Mochalin et al. 2009; Mermoux et al. 2014; Tarasenka et al. 2017). The resulting broad asymmetric peak showed a low signal-to-noise ratio. In fact, the reason for this observation is rather strong fluorescence, which agrees with the results of PL studies on nanocolloids. An analysis of the Raman spectrum shows a typical feature of nanostructured materials, which is the redshift of the *D* band, by 50 cm^{-1}, as compared with the literature data (Smith and Godard 2009).

According to TGA data (Fig. 2c), the FON-CNPs are stable below 200 °C, and the total weight loss of 52.7% is because of the thermal decomposition and detachment of the surface groups and the partial burning of the carbon shell. The content of physisorbed molecules, which are desorbed below 140 °C, is negligible, only 0.4%. The differential thermal gravimetric (DTG) curve revealed three main weight loss peaks at 365 °C, 533 °C, and 1096 °C. Here, the effect at 533 °C has a complex nature, and one can see the shoulder on the DTG curve between 650 °C and 800 °C. Actually, the

first and second weight loss effects are difficult to separate precisely. If they are separated by the temperature corresponding to the smallest weight change (of about 476 °C), the effect peaked at 365 °C will give 19.6% weight loss, while the effect at 533 °C–23.3% weight loss. The third effect at 1096 °C corresponds to 9.4% weight loss. From the above consideration, the schematic of the synthesis and the suggested products are depicted in Fig. 3.

At the first stage of the synthesis, aniline reacts with urea and citric acid, as a result, thermolysis products are formed and water is split off (Fig. 3a). It is likely that heterocyclic nitrogen-containing compounds are formed due to thermolytic condensation when citric acid reacts with urea (Fig. 3b). At a further stage, thermolysis products can participate in the construction of a growing carbon particle, enriching it with nitrogen atoms and trifluoromethyl groups.

**The aqueous solution of the FON-CNPs is yellowish and transparent under sunlight illumination. Figure. 4a shows two specific absorption peaks at 246 and 350 nm (Fig. 4a), attributed to the π–π* (aromatic C=C) and *n*–π* (the C=O bond) transitions according to Wang et al. (2017). Furthermore, according to Shen et al. (2013), Xiang et al. (2018), and Ding et al. (2016), the observed short- and long-wavelength absorption bands, at ca. 277 nm and at 435 nm and ca. 511 nm, can be attributed to the π → π* (aromatic C=C) and n → π* (C–N) transitions of nitrogen-containing groups in the FON-CNPs, respectively. To consider the effect of constitutional (structural heterocyclic) nitrogen and the active surface functional groups, we examined the response of FON-CNPs to various pH conditions in the PB buffer with variable pH values (Fig. 4b). At a wavelength of 212 nm, the FON-CNPs have a good response

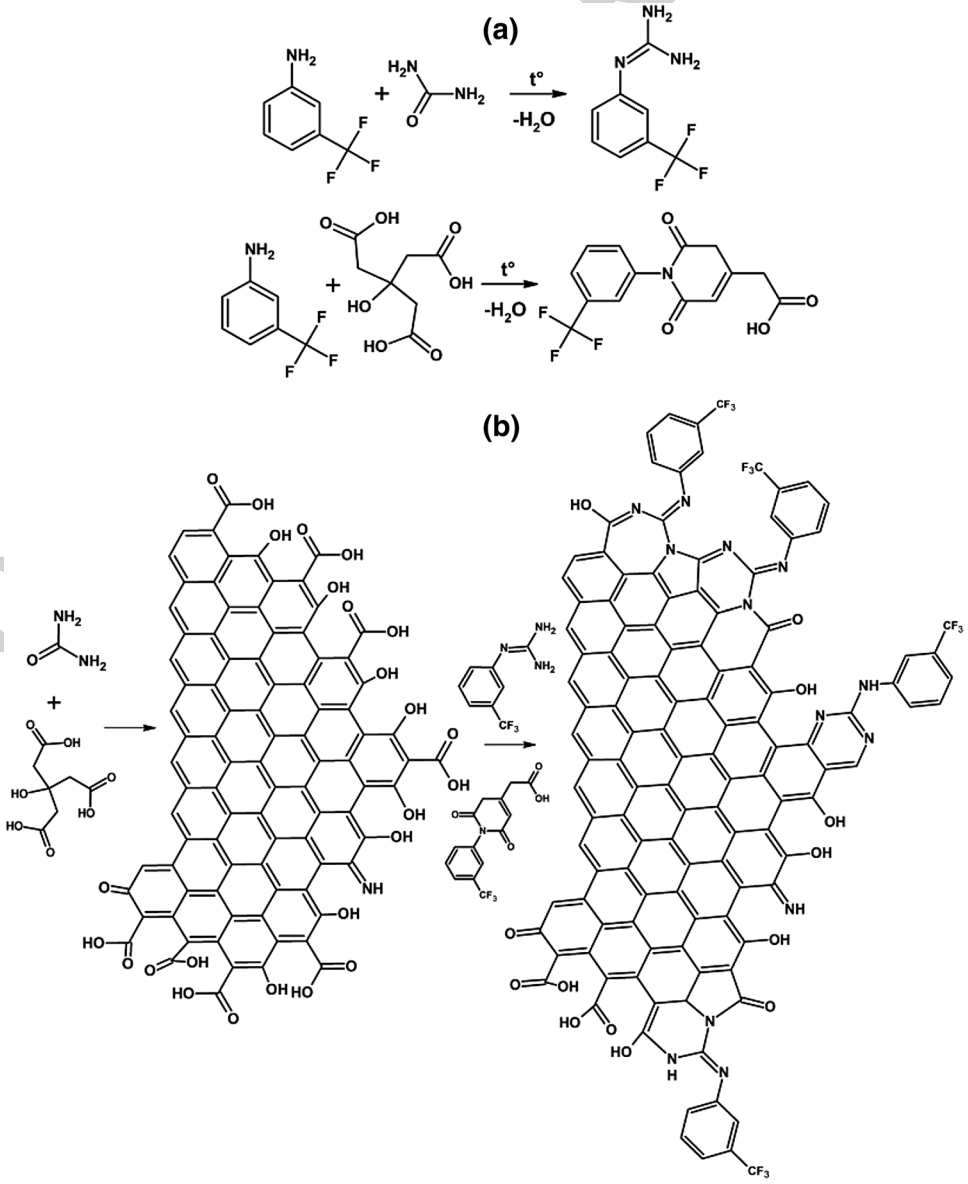

Fig. 3 Schematic illustration of FON-CNPs synthesis **a** thermolysis and **b** thermolytic condensation

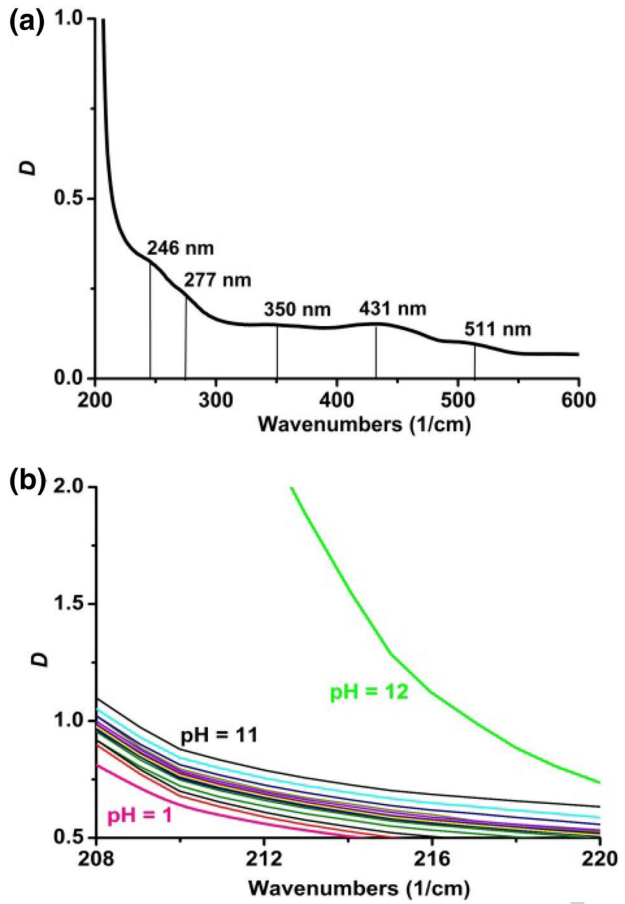

Fig. 4 **a** UV–Vis spectrum of FON-CNPs in water solution (0.03 mass%) and **b** pH-dependent response of FON-CNPs in different pHs (from top to bottom)

to the pH range from 1 to 6. In the absorbance (D) range from 0.55 to 0.75, $pH = (31.87 \pm 2.1)\ D - 16.89 \pm 1.3$ with $R^2 = 0.99$. At the same wavelength, the UV–vis spectra of FON-CNPs solutions also showed a linear response, in the D range of 0.71–0.8, to the pH ranged from 8 to 11: $pH = (28.11 \pm 1.56)D - 11.65 \pm 1.2$ with $R^2 = 0.99$.

The prepared FON-CNPs in solutions showed high tolerance to possible changes in the ionic strength. In fact, the PL intensity showed good stability in solutions with up to 1.0 mol L^{-1} NaCl. These solutions have good resistance to photobleaching, and the PL intensity remains constant under continuous irradiation for 2 h. We suggest that FON-CNPs can find potential applications in bio-labeling/bio-imaging. Moreover, the hydrogen bonds of the shell and steric protection of C–F bonds reduce photoluminescence quenching at room temperature.

On the other hand, the PL features of the prepared FON-CNPs are highly pH-dependent (Fig. 5). This observation indicates that PL species in the FON-CNPs should have basic/acidic sites taking part in reversible protonation and responsible for the PL intensity variation. We assume that the pH level increasing caused the negative surface charging; the de-protonation can dissociate hydrogen bonds. It will be a reason for the dissociation of both amide groups and carboxylic groups, in the background of possible deprotonating of nitrogen-containing groups (Long et al. 2018).

As shown in Fig. 4, as pH increased from 3.0 to 10.0, a gradient increase of the PL intensity of FON-CNPs centered at 510–525 nm can be seen. This increase of the PL intensity remained relatively steady in the 9.0–10.0 pH range (Fig. 5a–e). However, the PL signal peak is slightly red-shifted from 510 to 525 nm when the pH values increased from 3.0 to 11.0. The specific features, the blue shift to 475 nm and the PL signal quenching was registered when pH values in the colloid solutions increased from 10.0 to 12.0 (see Fig. 5e–g). As can be seen from Fig. 5, the prepared FON-CNPs could be sensitive pH indicators due to their pH-dependent PL intensity. Additionally, there is a good linear relationship between the PL intensity and the pH of solutions in the range of 3.0–9.0, the relationship between the PL intensity and pH values was fitted as a linear equation of $PL(a.u.) = (16.76 \pm 2.2)[pH] + 769.0 \pm 20$ with $R^2 = 0.99$. But the PL response deviates from linearity in the higher and lower ranges.

An alternative view on the pH-sensing mechanism could be formulated considering the chemistry of FON-CNPs. If judging by the TG data, the prepared FON-CNPs are rich in carboxyl groups and other oxygen functionality (phenolic and carbonyl groups).

With an increase in pH, the carboxyl groups are first deprotonated. This de-protonation can increase the luminescence with the concentration of ionized particles in the solution. At high basic pH levels, we observe some quenching of luminescence. One can explain this observation by the ionization of the carbonyl functional group. The latter is typical for dyes at such high pH values. Apparently, the ionization of the carbonyl groups leads to the destruction of conjugated systems inside the matrix and, accordingly, results in the quenching of the PL signal.

Conclusion

The core–shell FON-CNPs prepared using trifluoromethylated derivatives were found to be excellent PL probes for pH measurements. We consider possible reasons for the pH-sensitive PL enhancement and PL subsequent quenching in the solutions of FON-CNPs. It has been demonstrated that the FON-CNPs have a good linearity range in the detection of pH levels. The reported sensing system based on the PL response of FON-CNPs shows many advantages, including rapid detection, high sensitivity, and medium–low production costs of the probe FON-CNPs. Potentially, as high

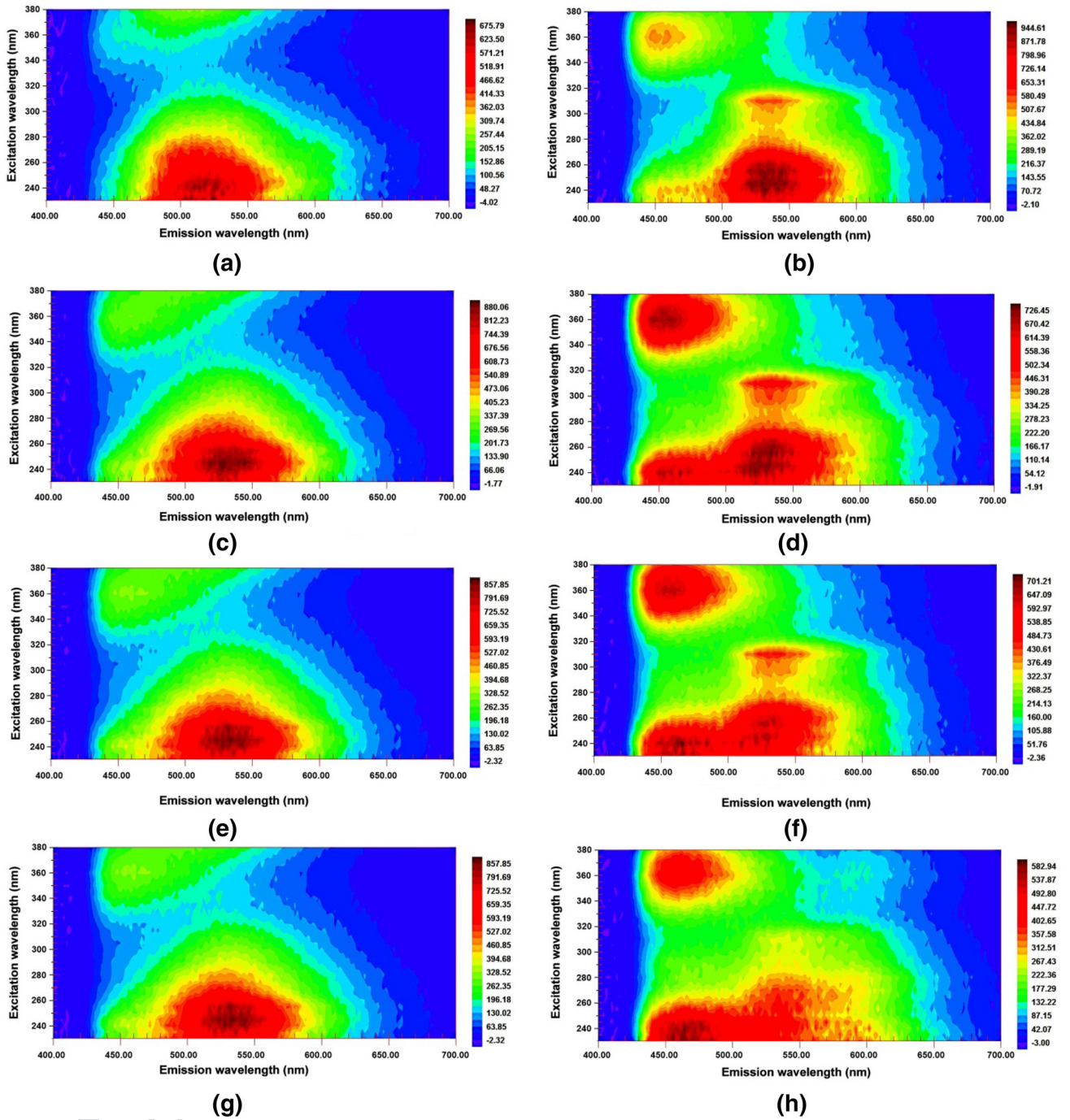

Fig. 5 3D PL plots of selected aqueous solution of FON-CNPs in different pHs: **a** 1.07, **b** 5.32, **c** 6.17, **d** 9.03, **e** 9.81, **f** 10.13, **g** 10.73, and **h** 12.03

selective probes, they can be applied to measure pH levels in aqueous solutions and cells.

Acknowledgements G.K. Mussabek, Y.T. Taurbayev, and V.V. Lisnyak acknowledge the support of Grant No AP08856579 of the Ministry of Education and Science of the Republic of Kazakhstan. G.K. Mussabek is grateful to Al-Farabi Kazakh National University for a Scholarship in the Postdoctoral Fellowship program. A.N. Zaderko and V.A. Skryshevsky recognize a support from the Ministry of Education and Science of Ukraine, Grant No 0119U100326. A.N. Zaderko is also thankful for the scholarship of the National Scholarship Programme of the Slovak Republic, Grant No 32492. This work was partially supported by EU Horizon 2020 Research and Innovation Staff Exchange Programme (RISE) under Marie Skłodowska-Curie Action (project 101008159 "UNAT").

Compliance with ethical standards

Conflict of interest A.N. Zaderko is the inventor of the WO2020121119 international patent publication. A.N. Zaderko is the owner of the trademark Fluocar® Nano UA213198 and US5479088. All authors declare that they have no conflict of interest.

References

Bellamy LJ (1980) Carbonyl Frequencies. In: Bellamy LJ (ed) The infrared spectra of complex molecules. Springer, Dordrecht, pp 128–194

Benilov A, Gavrilchenko I, Benilova I, Skryshevsky V, Cabrera M (2007) Influence of pH solution on photoluminescence of porous silicon. Sens Actuators A 137:345–349. https://doi.org/10.1016/j.sna.2007.02.032

Cançado LG, Takai K, Enoki T, Endo M, Kim YA et al (2006) General equation for the determination of the crystallite size La of nanographite by Raman spectroscopy. Appl Phys Lett 88:163106. https://doi.org/10.1063/1.2196057

Coates J (2006) Interpretation of infrared spectra a practical approach. In: Meyers RA, McKelvy ML (eds) Encyclopedia of analytical chemistry. Wiley, Hoboken

Soc C, Inc. (2018) Evaluated Infrared Reference Spectra. In: Linstrom PJ, Mallard WG (eds) NIST chemistry webbook, nist standard reference database number 69. National Institute of Standards and Technology, Gaithersburg

Ding H, Yu SB, Wei JS, Xiong HM (2016) Full-color light-emitting carbon dots with a surface-state-controlled luminescence mechanism. ACS Nano 10:484–491. https://doi.org/10.1002/adma.201704740

Feng S, Mu Z, Liu H et al (2019) A novel application of fluorine doped carbon dots combining vortex-assisted liquid-liquid microextraction for determination of 4-nitrophenol with spectrofluorimetric method. J Fluoresc 29:1133–1141. https://doi.org/10.1007/s10895-019-02427-8

He J, Chen Y, He Y, Xu X (2020) Anchoring carbon nanodots onto nanosilica for phosphorescence enhancement and delayed fluorescence nascence in solid and liquid states. Small 16:49. https://doi.org/10.1002/smll.202005228

Jiang L, Ding H, Lu S, Geng T et al (2019) Photoactivated fluorescence enhancement in F, N-doped carbon dots with piezochromic behavior. Angew Chem 132:10072–10077. https://doi.org/10.1002/ange.201913800

Kauffman KL, Culp JT, Goodman A, Matranga C (2011) FT-IR study of CO_2 adsorption in a dynamic copper (II) benzoate-pyrazine host with CO_2–CO_2 interactions in the adsorbed state. J Phys Chem C 115:1857–1866. https://doi.org/10.1021/jp102273w

Larkin PJ (2011) Infrared and Raman spectroscopy principles and spectral interpretation. Elsevier, Amsterdam, pp 61–62

Lin-Vien D, Colthup NB, Fateley WG, Grasselli JG (1991) The handbook of infrared and Raman characteristic frequencies of organic molecules. Academic Press, San Diego, pp 479–481

Lin C-K (2018) Pyridine vs. N-Hydrogenated pyridine moieties: theoretical study of stability and spectroscopy of nitrogen-contained heterocyclic aromatic compounds and graphene nanoflakes. ACS Omega 3:12312–12319. https://doi.org/10.1021/acsomega.8b01759

Liu L, Anwar S, Ding H, Xu M (2019) Electrochemical sensor based on F, N-doped carbon dots decorated laccase for detection of catechol. J Electroanal Chem 840:84–92. https://doi.org/10.1016/j.jelechem.2019.03.071

Long P, Feng Y, Cao C, Li Y et al (2018) Self-protective room-temperature phosphorescence of fluorine and nitrogen codoped carbon dots. Adv Funct Mater 28:1800791. https://doi.org/10.1002/adfm.201800791

Mermoux M, Crisci A, Petit T, Girard HA, Arnault J-C (2014) Surface modifications of detonation nanodiamonds probed by multiwavelength Raman spectroscopy. J Phys Chem C 118:23415–23425. https://doi.org/10.1021/jp507377z

Mochalin V, Osswald S, Gogotsi Y (2009) Contribution of functional groups to the Raman spectrum of nanodiamond. Chem Mater 21:273–279. https://doi.org/10.1021/cm802057q

Nevar A, Tarasenka N, Nedelko M, Tarasenko N (2020) Carbon nanodots with tunable luminescence properties synthesized by electrical discharge in octane. Carbon Lett. https://doi.org/10.1007/s42823-020-00147-9

Novoa De León IC, Johny J, Vázquez-Rodríguez S, García-Gómez N, Carranza-Bernal S, Mendivil I, Shaji S, Sepúlveda-Guzmán S (2019) Tuning the luminescence of nitrogen-doped graphene quantum dots synthesized by pulsed laser ablation in liquid and their use as a selective photoluminescence on–off–on probe for ascorbic acid detection. Carbon 150:455–464. https://doi.org/10.1016/j.carbon.2019.05.057

Pal A, Sk MP, Chattopadhyay A (2020) Recent advances in crystalline carbon dots for superior application potential. Mater Adv 1:525–553. https://doi.org/10.1039/D0MA00108B

Rap DB, Marimuthu AN, Redlich B, Brünken S (2020) Stable isomeric structures of the pyridine cation ($C_5H_5N\bullet^+$) and protonated pyridine ($C_5H_5NH^+$) elucidated by cold ion infrared spectroscopy. J Mol Spectrosc 373:111357. https://doi.org/10.1016/j.jms.2020.111357

Serdiuk T, Skryshevsky VA, Ivanov II, Lysenko V (2011) Storage of luminescent nanoparticles in porous silicon: toward a solid state "golden fleece." Mater Lett 65:2514–2517. https://doi.org/10.1016/j.matlet.2011.05.033

Shahravan A, Desai T, Matsoukas T (2012) Controlled manipulation of wetting characteristics of nanoparticles with dry-based plasma polymerization method. Appl Phys Lett 101:251603. https://doi.org/10.1063/1.4772544

Shen L, Zhang L, Chen M, Chen X, Wang J (2013) The production of pH-sensitive photoluminescent carbon nanoparticles by the carbonization of polyethylenimine and their use for bioimaging. Carbon 55:343–349. https://doi.org/10.1016/j.carbon.2012.12.074

Sim Y, Seung Kim SJ, Janani G, Chae Y et al (2019) The synergistic effect of nitrogen and fluorine co-doping in graphene quantum dot catalysts for full water splitting and supercapacitor. Appl Surf Sci 50:145157. https://doi.org/10.1016/j.apsusc.2019.145157

Singh NP, Yadav RA (2001) Vibrational studies of trifluoromethyl benzene derivatives 1: 2-amino, 5-chloro and 2-amino. 5-bromo benzotrifluorides. Indian J Phys 75B:347–355

Smith DC, Godard G (2009) UV and VIS Raman spectra of natural lonsdaleites: towards a recognised standard. Spectrochim Acta A 73:428–435. https://doi.org/10.1016/j.saa.2008.10.025

Socrates G (1994) Infrared characteristic group frequencies. Wiley, New York

Su Q, Lu C, Yang X (2019) Efficient room temperature phosphorescence carbon dots: Information encryption and dual-channel pH sensing. Carbon 152:609–615. https://doi.org/10.1016/j.carbon.2019.06.061

Sun Y, Liu S, Sun L, Wu S et al (2020) Ultralong lifetime and efficient room temperature phosphorescent carbon dots through multi-confinement structure design. Nature Commun 11:1. https://doi.org/10.1038/s41467-020-19422-4

Tarasenka N, Stupak A, Tarasenko N, Chakrabarti S, Mariotti D (2017) Structure and optical properties of carbon nanoparticles generated by laser treatment of graphite in liquids. ChemPhysChem 18:1074. https://doi.org/10.1002/cphc.201601182

Tsapyuk GG, Diyuk VE, Mariychuk R et al (2020) Effect of ultrasonic treatment on the thermal oxidation of detonation nanodiamonds. Appl Nanosci 10:4991–5001. https://doi.org/10.1007/s13204-020-01277-2

Wang H, Sun C, Chen X, Zhang Y et al (2017) Excitation wavelength independent visible color emission of carbon dots. Nanoscale 9:1909–1915. https://doi.org/10.1039/C6NR09200D

Wang Y, Yue Q, Hu Y, Liu C et al (2019) Synthesis of N-doped carbon dots and application in vanillin detection based on collisional quenching. RSC Adv 9:40222–40227. https://doi.org/10.1039/C9RA08352A

Xia C, Zhu S, Feng T, Yang M, Yang B (2019) Evolution and synthesis of carbon dots: from carbon dots to carbonized polymer dots. Adv Sci 6:23. https://doi.org/10.1002/advs.201901316

Xiang M, Dan Q, Dongxue Y, Bing N, Yikang Z, Hongyou F, Zaicheng S (2018) Synthesis of carbon dots with multiple color emission by controlled graphitization and surface functionalization. Adv Mater 30:1704740. https://doi.org/10.1021/acsnano.5b05406

Yadav RA, Singh IS (1985) Vibrational spectra and normal coordinate analysis for substituted trifluoromethyl benzenes. Proc Indian Acad Sci (Chem Sci) 95:471–487. https://doi.org/10.1007/BF02840446

Yang P, Zhu Z, Chen W, Luo M et al (2020) Nitrogen/sulfur Co-doping strategy to synthesis green-yellow emitting carbon dots derived from xylose: toward application in pH sensing. J Lumin 232:117489. https://doi.org/10.1016/j.jlumin.2020.117489

Zaderko A (2020) The process for obtaining of fluoralkylated carbon quantum dots. WO2020121119 Patent. https://patentscope.wipo.int/search/en/detail.jsf?docId=WO2020121119. Accessed 25 Jan 2021

Zaderko AN, Shvets RYa, Grygorchak II et al (2019) Fluoroalkylated nanoporous carbons: testing as a supercapacitor electrode. Appl Surf Sci 470:882–892. https://doi.org/10.1016/j.apsusc.2018.11.141

Zan M, Li C, Liao F, Rao L et al (2020) One-step synthesis of green emission carbon dots for selective and sensitive detection of nitrite ions and cellular imaging application. RSC Adv 10:10067–10075. https://doi.org/10.1039/C9RA11009G

Zuo G, Xie A, Pan X, Su T, Li J, Dong W (2018) Fluorine-doped cationic carbon dots for efficient gene delivery. ACS Appl Nano Mater 1(5):376–2385. https://doi.org/10.1021/acsanm.8b00521

Journal:	**13204**
Article:	**1725**

Author Query Form

Please ensure you fill out your response to the queries raised below and return this form along with your corrections

Dear Author

During the process of typesetting your article, the following queries have arisen. Please check your typeset proof carefully against the queries listed below and mark the necessary changes either directly on the proof/online grid or in the 'Author's response' area provided below

Query	Details Required	Author's Response
AQ1	Author names: Please confirm if the author names are presented accurately and in the correct sequence (given name, middle name/initial, family name). Also, kindly confirm the details in the metadata are correct.	